Time Discrete Extrapolation in a Riemannian Space of Images

Alexander Effland[1], Martin Rumpf[1], and Florian Schäfer[2]

[1] Institute for Numerical Simulation, Universität Bonn,
{alexander.effland, martin.rumpf}@ins.uni-bonn.de
[2] California Institute of Technology,
florian.schaefer@caltech.edu

Abstract. The Riemannian metamorphosis model introduced and analyzed in [8,13] is taken into account to develop an image extrapolation tool in the space of images. To this end, the variational time discretization for the geodesic interpolation proposed in [2] is picked up to define a discrete exponential map. For a given weakly differentiable initial image and a sufficiently small initial image variation it is shown how to compute a discrete geodesic extrapolation path in the space of images. The resulting discrete paths are indeed local minimizers of the corresponding discrete path energy. A spatial Galerkin discretization with cubic splines on coarse meshes for image deformations and piecewise bilinear finite elements on fine meshes for image intensity functions is used to derive a fully practical algorithm. The method is applied to real images and image variations recorded with a digital camera.

Keywords: image extrapolation, shape space, elastic registration, exponential map

1 Introduction

Riemannian geometry has influenced imaging and computer vision tremendously in the past decades. In particular, many methods in image processing have benefited from concepts emerging from Riemannian geometry like geodesic curves, the logarithm, the exponential map, and parallel transport. For example, when considering the space of images as an infinite-dimensional Riemannian manifold, the exponential map of an input image w.r.t. an initial variation corresponds to an image extrapolation in the direction of this infinitesimal variation. In particular, the large deformation diffeomorphic metric mapping (LDDMM) framework proved to be a powerful tool underpinned with the rigorous mathematical theory of diffeomorphic flows. In fact, Dupuis et al. [3] showed that the resulting flow is actually a flow of diffeomorphism. Trouvé [11] exploited Lie group methods to construct a distance in the space of deformations. Vialard et al. [14,15] studied methods from optimal control theory to accurately estimate this initial momentum and to relate it to the Hamiltonian formulation of the geodesic flow. Furthermore, they used the associated Karcher mean to compute intrinsic means of medical images. Lorenzi and Pennec [7] applied the LDDMM framework to compute geodesics and parallel transport using Lie group methods.

The metamorphosis model [8,13] generalizes the flow of diffeomorphism approach allowing for intensity variations along transport paths and associated a corresponding cost functional with these variations. In [12], Trouvé and Younes rigorously analyzed the local geometry of the resulting Riemannian manifold and proved the existence of geodesic curves for square-integrable images and the (local) existence as well as the uniqueness of solutions of the initial value problem for the geodesic equation in the case of images with square-integrable weak derivatives. Holm et al. [5] studied a Lagrangian formulation for the metamorphosis model and proved existence both for the boundary value and the initial value problem in the case of measure-valued images.

In [2], a variational time discretization of the metamorphosis model based on a sequence of simple, elastic image matching problems was introduced and Γ-convergence to the time continuous metamorphosis model was proven. Furthermore, using a finite element discretization in space a robust algorithm was derived.

Here, we pick up this approach and use it to develop a discrete exponential map in the space of images. In fact, the Euler-Lagrange equations of the discrete path energy proposed in [2] give rise to a set of equations, which characterize time steps of a discrete initial value problem for a given initial image and a given initial image variation. A straightforward treatment, for instance via a Newton scheme, would lead to higher order derivatives of image functions concatenated with diffeomorphic deformations, which are both theoretically and numerically very difficult to treat. We show how to avoid these difficulties using a proper transformation of the defining Euler-Lagrange equations via integral transformations, integration by parts, and suitable choices of test functions, and reduce the number of unknowns. To this end, we derive a fixed point algorithm based on a suitable variant of the Euler-Lagrange equations.

The paper is organized as follows: In Section 2, we briefly recall the metamorphosis model in the time continuous and time discrete setting, respectively. Departing from the Euler-Lagrange equations of a time discrete geodesic, a single time step of the discrete exponential map is derived in Section 3. Then the discrete geodesic shooting relies on the iterative application of the one step extrapolation. In Section 4, the associated Euler-Lagrange equations are rewritten as a fixed point problem. Using suitable discrete ansatz spaces an efficient and stable algorithm is derived in Section 5. Finally, numerical results for different applications are presented in Section 6.

2   Review of the metamorphosis model and its time discretization

In this section, we briefly recall in a non-rigorous fashion the Riemannian geometry of the space of images based on the flow of diffeomorphism and its extension, the metamorphosis model. For a detailed exposition of these models we refer to [3,8,13,5,12].

Throughout this paper, we suppose that the image domain $\Omega \subset \mathbb{R}^n$ for $n \in \{2,3\}$ has Lipschitz boundary. For a flow of diffeomorphism $\phi(t) : \bar{\Omega} \to \mathbb{R}^n$ for $t \in [0,1]$ driven by the *Eulerian velocity* $v(t) = \dot{\phi}(t) \circ \phi^{-1}(t)$ we take into account a quadratic form L subjected to certain growth and consistency conditions, which can be considered as a Riemannian metric on the space of diffeomorphisms and thus on the space of diffeomorphic transformations $u(t) = u_0 \circ \phi^{-1}(t)$ of a given reference image u_0. Based

on these ingredients one can define the associated *(continuous) path energy*

$$\widetilde{\mathcal{E}}[(\phi(t))_{t\in[0,1]}] = \int_0^1 \int_\Omega L[v,v]\,\mathrm{d}x\,\mathrm{d}t\,.$$

By construction, this model comes with the brightness constancy assumption in the sense that the material derivative $\frac{D}{\partial t}u = \dot{u}+v\cdot\nabla u$ vanishes along the motion paths. Contrary to this, the metamorphosis approach allows for image intensity variations along motion paths and penalizes the integral over the squared material derivative as an additional term in the metric. Hence, the *path energy* in the metamorphosis model for an image curve $u \in L^2((0,1), L^2(\Omega))$ and $\delta > 0$ is defined as

$$\mathcal{E}[u] := \int_0^1 \inf_{(v,z)} \int_\Omega L[v,v] + \frac{1}{\delta}z^2\,\mathrm{d}x\,\mathrm{d}t\,, \qquad (1)$$

where the infimum is taken over all pairs $(v,z) \in H_0^{2m}(\Omega, \mathbb{R}^n) \times L^2(\Omega, \mathbb{R})$ which fulfill the transport equation $\frac{D}{\partial t}u = \dot{u} + v \cdot \nabla u = z$. Here, we consider $L[v,v] := Dv : Dv + \gamma\Delta^m v \cdot \Delta^m v$ with $\gamma > 0$ and $2m > 1 + \frac{n}{2}$, where we use the notation $A : B = \mathrm{tr}(A^T B)$. To formulate this rigorously, one has to take into account the weak material derivative $z \in L^2((0,1), L^2(\Omega))$ defined via the equation $\int_0^1 \int_\Omega \eta z\,\mathrm{d}x\,\mathrm{d}t = -\int_0^1 \int_\Omega (\partial_t\eta + \mathrm{div}(v\eta))u\,\mathrm{d}x\,\mathrm{d}t$ for all $\eta \in C_c^\infty((0,1) \times \Omega)$. Geodesic curves are defined as minimizers of the path energy (1). Under suitable assumptions, one can prove the existence of a *geodesic curve* in the class of all regular curves with prescribed initial and end image. For the definition of regular curves and the existence proof we refer to [12].

In what follows, we consider the time discretization of the path energy (1) proposed in [2] adapted to the slightly simpler transport cost $L[\,\cdot\,,\,\cdot\,]$. To this end, we define for arbitrary images $u, \tilde{u} \in L^2(\Omega)$ the *time discrete matching energy*

$$\mathcal{W}[u,\tilde{u}] := \min_{\phi\in\mathcal{A}}\left\{\mathcal{W}^D[u,\tilde{u},\phi] := \int_\Omega |D\phi - \mathbb{1}|^2 + \gamma|\Delta^m\phi|^2 + \frac{1}{\delta}(\tilde{u}\circ\phi - u)^2\,\mathrm{d}x\right\}, \quad (2)$$

which is composed of a rescaled thin plate regularization term (first two terms) and a quadratic $L^2(\Omega)$-mismatch measure (cf. [2, (6.2)]). Here, we define the *set of admissible deformations* $\mathcal{A} := \left\{\phi \in H^{2m}(\Omega, \Omega) : \phi - \mathbb{1} \in H_0^{2m}(\Omega, \Omega)\right\}$.

Using the direct method in the calculus of variations it is easy to show that for $u \in L^2(\Omega)$ and $2m - \frac{n}{2} > 1$, which ensures the continuity of the deformations via Sobolev embedding, there exists a constant $C_\mathcal{W} > 0$ that solely depends on γ, δ, Ω and m, such that for every $\tilde{u} \in L^2(\Omega)$ with $\|\tilde{u} - u\|_{L^2(\Omega)} \leq C_\mathcal{W}$ there is a minimizing deformation $\phi \in \mathcal{A}$ for $\mathcal{W}$, i.e. $\mathcal{W}[u,\tilde{u}] = \mathcal{W}^D[u,\tilde{u},\phi]$, and ϕ is a $C^1(\Omega)$-diffeomorphism.

Following the general approach for the variational time discretization of geodesic calculus in [10] and the particular discretization of the metamorphosis model in [2], we define the discrete path energy $\mathbf{E}_K$ on a sequence of $K + 1$ images $(u_0, \ldots, u_K) \in (L^2(\Omega))^{K+1}$ with $K \geq 2$ as the weighted sum of the discrete matching energy evaluated at consecutive images, i.e.

$$\mathbf{E}_K[u_0, \ldots, u_K] := K\sum_{k=1}^K \mathcal{W}[u_{k-1}, u_k]\,. \qquad (3)$$

Then, a $(K+1)$-tuple $(u_0, \ldots, u_K) \in (L^2(\Omega))^{K+1}$ with given images u_0 and u_K is defined to be a *discrete geodesic curve* connecting u_0 and u_K if it minimizes $\mathbf{E}_K$ w.r.t. all other $(K+1)$-tuples with u_0 and u_K fixed. It is shown in [2] that a suitable extension of the discrete path energy $\mathbf{E}_K$ Γ-convergences to the continuous path energy $\mathcal{E}$. Let us finally mention that neither the matching deformation in (2) nor the discrete geodesic curve defined as the minimizer of (3) for given input images u_0 and u_K are necessarily unique.

3   The time discrete exponential map

Before we define the discrete exponential map let us briefly recall the definition of the continuous exponential map on a Riemannian manifold. Let $y : [0,1] \to \mathcal{M}$ be the unique geodesic curve for a prescribed initial position $y(0) = y_A$ and an initial velocity $\dot{y}(0) = v$ on a Riemannian manifold $(\mathcal{M}, g)$. The exponential map is then defined as $\exp_{y_A}(v) = y(1)$. Furthermore, one easily checks that $\exp_{y_A}(\frac{k}{K}v) = y(\frac{k}{K})$ for $0 \le k \le K$. We refer to the textbook [6] for a detailed discussion of the (continuous) exponential map. Now, we ask for a time discrete counterpart of the exponential map in the metamorphosis model. To this end, we consider an image u_0 as the initial data and a second image u_1 such that $\zeta_1 = u_1 - u_0$ represents a small variation of the image u_0. This variation ζ_1 is the discrete counterpart of the infinitesimal variation given by the velocity v in the continuous case. For varying values of $K \ge 2$ we now ask for a discrete geodesic $(u_0, u_1, \ldots, u_K)$ defined as the minimizer of the discrete path energy (3). For simplicity, let us suppose that this discrete geodesic curve is unique, which is indeed true for short discrete geodesics. Based on our above observation for the continuous exponential map we then define $\mathrm{EXP}_*^k(\,\cdot\,)$ as the discrete counterpart of $\exp_*(\frac{k}{K}\,\cdot\,)$, i.e. we set

$$\mathrm{EXP}_{u_0}^k(\zeta_1) := u_k$$

for $k = 1, \ldots, K$. The definition of the exponential map $\mathrm{EXP}_{u_0}^k(\zeta_1)$ does not depend on the number of time steps K. Indeed, if $(u_0, u_1, u_2, \ldots, u_K)$ is a discrete geodesic, then $(u_0, u_1, u_2, \ldots, u_k)$ with $k \le K$ is also a geodesic. Taking into account $k = 2$ we immediately observe that the sequence of discrete exponential maps $(\mathrm{EXP}_{u_0}^k(\zeta_1))_{k=1,\ldots}$ can iteratively be defined as follows

$$\mathrm{EXP}_{u_0}^k(\zeta_1) = u_k := \mathrm{EXP}_{u_{k-2}}^2(\zeta_{k-1}) \tag{4}$$

for $k \ge 2$, where $\zeta_{k-1} = u_{k-1} - u_{k-2}$, and for the sake of completeness we define $\mathrm{EXP}_{u_0}^0(\zeta_1) = u_0$ and $\mathrm{EXP}_{u_0}^1(\zeta_1) = u_1 = u_0 + \zeta_1$. Thus, it essentially remains to compute EXP^2 for a given input image u_{k-2} and an image variation $\zeta_{k-1} = u_{k-1} - u_{k-2}$ (see Figure 1). For a detailed discussion of the discrete exponential map in the simpler model of Hilbert manifolds we refer to [10]. The particular challenge here is that the matching energy $\mathcal{W}$ cannot be evaluated directly, but requires to solve the variational problem (2) for the matching deformation.

There are two major restrictions regarding the input images u_0 and u_1: we require input images with square-integrable weak derivatives and we assume that the initial variation is sufficiently small in $L^2(\Omega)$. Both properties are kept along the extrapolated

Fig. 1. Schematic drawing of $\mathrm{EXP}^k_{u_0}(\zeta_1)$, $k = 1, \dots, K$, the input data is highlighted in red.

image sequence, i.e. $\mathrm{EXP}^k_{u_0}(u_1 - u_0) \in H^1(\Omega)$ for any $k \geq 1$ and $u_{k-1} - u_{k-2}$ for $k \geq 2$ will remain small provided that ζ_1 is small.

Hence, in what follows we consider images in $H^1(\Omega)$ and define for any $k \geq 2$ $u_k := \mathrm{EXP}^2_{u_{k-2}}(\zeta_{k-1})$ as the (unique) image in $H^1(\Omega)$ such that

$$u_{k-1} = \operatorname*{argmin}_{u \in H^1(\Omega)} \min_{\phi_{k-1}, \phi_k \in \mathcal{A}} \mathcal{W}^D[u_{k-2}, u, \phi_{k-1}] + \mathcal{W}^D[u, u_k, \phi_k]. \tag{5}$$

For the sake of simplicity, we restrict to the first step in the iterative computation of the discrete exponential map with $k = 2$. Given $u_0, u_1 \in H^1(\Omega)$ the first order optimality conditions for (5) for $u_2 \in H^1(\Omega)$ and $\phi_1, \phi_2 \in \mathcal{A}$ read as

$$\int_\Omega (u_1 \circ \phi_1 - u_0)v \circ \phi_1 - (u_2 \circ \phi_2 - u_1)v \, \mathrm{d}x = 0, \tag{6}$$

$$\int_\Omega 2D\phi_1 : D\psi + 2\gamma\Delta^m\phi_1 \cdot \Delta^m\psi + \frac{2}{\delta}(u_1 \circ \phi_1 - u_0)(\nabla u_1 \circ \phi_1) \cdot \psi \, \mathrm{d}x = 0, \tag{7}$$

$$\int_\Omega 2D\phi_2 : D\psi + 2\gamma\Delta^m\phi_2 \cdot \Delta^m\psi + \frac{2}{\delta}(u_2 \circ \phi_2 - u_1)(\nabla u_2 \circ \phi_2) \cdot \psi \, \mathrm{d}x = 0 \tag{8}$$

for all $v \in H^1(\Omega)$ and all $\psi \in H^{2m}_0(\Omega)$ for $2m - \frac{n}{2} > 2$.

Next, we reformulate (8), remove the dependency on the unknown function u_2 and in addition restrict to function evaluations of u_1 and thereby avoid evaluations of derivatives of u_1. Under the assumptions that (6) and (7) hold true, $\partial\Omega \in C^{4m}$ and for $u_0, u_1, u_2 \in L^\infty(\Omega) \cap H^1(\Omega)$ equation (8) is equivalent to

$$\int_\Omega 2\gamma\Delta^m\phi_2 \cdot \Delta^m\psi + 2D\phi_2 : D\psi \, \mathrm{d}x =$$

$$\int_\Omega 2\gamma\Delta^m\phi_1 \cdot \Delta^m(((D\phi_2)^{-1}\psi) \circ \phi_1) + 2D\phi_1 : D(((D\phi_2)^{-1}\psi) \circ \phi_1)$$

$$- \frac{(u_1 \circ \phi_1 - u_0)^2}{\delta \det D\phi_1}\left((D\phi_2)^{-T} : (D^2\phi_2(D\phi_2)^{-1}\psi) - (D\phi_2)^{-T} : D\psi\right) \circ \phi_1 \, \mathrm{d}x. \tag{9}$$

The proof of this reformulation is based on a repeated application of the transformation formula and a regularity result for polyharmonic equations (see the appendix). We will use it to define a fully discrete fixed point iteration to compute the deformation ϕ_2 numerically. Once ϕ_2 is available the image u_2 can be calculated via the equation

$$u_2 = \left(\frac{u_1 - u_0 \circ \phi_1^{-1}}{\det(D\phi_1) \circ \phi_1^{-1}}\right) \circ \phi_2^{-1} + u_1 \circ \phi_2^{-1}, \tag{10}$$

which directly follows from (6) by the transformation rule taking into account the diffeomorphism property of ϕ_2. Here, the first summand reflects the intensity modulation along the geodesic, the second summand quantifies the contribution due to the transport.

Concerning a theoretical foundation of this approach, it can be shown that there exists a solution (u_2, ϕ_1, ϕ_2) to the system of equations (6), (7) and (8) for image pairs (u_0, u_1) provided that u_0 and u_1 are bounded in $H^1(\Omega)$ and sufficiently close in $L^2(\Omega)$. This does not necessarily imply that for given u_0 and u_1 the resulting discrete path (u_0, u_1, u_2) is the unique discrete geodesic connecting u_0 and u_2. However, if the images u_0 and u_1 are sufficiently close in $H^1(\Omega)$, then a unique discrete geodesic connecting u_0 and u_2 exists. Existence can be established using a variant of the above fixed point argument and uniqueness under the stronger assumptions can be established by an implicit function theorem argument (cf. the corresponding proof for the discrete exponential map on Hilbert manifolds given in [10]). The presentation of the proofs goes beyond the scope of this paper.

4   Fixed point formulation

In what follows, we introduce a spatial discretization scheme as well as an algorithm to compute the discrete exponential map based on the time discrete operator $\mathrm{EXP}_{u_0}^2(u_1 - u_0)$ for given images u_0 and u_1. Let us recall that the computation of EXP^k for $k > 2$ requires the iterative application of EXP^2 as defined in (4). In explicit, we ask for a numerical approximation of the matching deformations ϕ_1, ϕ_2 and the current succeeding image $u_2 = \mathrm{EXP}_{u_0}^2(u_1 - u_0)$ along the (extrapolated) discrete path. Here, we restrict to two dimensional images and for the sake of simplicity we assume that the image domain is the unit square, i.e. $\Omega = (0, 1)^2$. Conceptually, the generalization to three dimensions is straightforward. As a simplification for the numerical implementation, we restrict to the case $m = 1$ despite the theoretical requirement that $m > 1 + \frac{n}{4} = \frac{3}{2}$.

To set up the fixed point iteration in light of (9) we define a nonlinear operator $\mathcal{T} : \mathcal{A} \to H^{-2m}(\Omega)$ and a linear operator $\mathcal{R} : \mathcal{A} \to H^{-2m}(\Omega)$ with

$$\mathcal{T}[\phi](\psi) = \int_\Omega -2\gamma D\Delta\phi_1 : (D((D\phi)^{-1}\psi) \circ \phi_1) - 2\Delta\phi_1 \cdot ((D\phi)^{-1}\psi) \circ \phi_1$$
$$- \frac{(u_1 \circ \phi_1 - u_0)^2}{\delta \det D\phi_1} \left((D\phi)^{-T} : (D^2\phi(D\phi)^{-1}\psi) - (D\phi)^{-T} : D\psi\right) \circ \phi_1 \, \mathrm{d}x$$

$$\mathcal{R}[\phi](\psi) = \int_\Omega 2\gamma\Delta^m\phi \cdot \Delta^m\psi + 2D\phi : D\psi \, \mathrm{d}x$$

for all $\psi \in H_0^{2m}(\Omega)$. The linear operator $\mathcal{R}$ has a bounded inverse by means of the Lax-Milgram theorem. Thus, we can rewrite (9) as a fixed point equation as follows

$$\phi_2 = \left(\mathcal{R}^{-1} \circ \mathcal{T}\right)[\phi_2] \tag{11}$$

and more explicitly $\mathcal{T}[\phi_2](\psi) = \mathcal{R}[\phi_2](\psi)$ for all test functions $\psi \in H_0^{2m}(\Omega)$. A core property of this formulation is that it does not require any evaluation of image intensity gradients. To improve the stability of the numerical algorithm with respect to

the evaluation of the first integrand of $\mathcal{T}[\phi](\psi)$ we additionally rewrite this expression by making use of $A : B = \mathrm{tr}(A^T B)$ as follows

$$\int_\Omega D\Delta\phi_1 : D((D\phi)^{-1}\psi) \circ \phi_1) \, \mathrm{d}x$$

$$= \int_\Omega ((D\phi)^{-T} \circ \phi_1)D\Delta\phi_1 : D(\psi \circ \phi_1) + D\Delta\phi_1 : D((D\phi)^{-1} \circ \phi_1)(\psi \circ \phi_1) \, \mathrm{d}x \,.$$

5 Space discretization

We use different discrete ansatz spaces for the deformations and the images reflecting the different regularity requirements of the fixed point formulation (11). As the discrete ansatz space for the deformations we choose the conforming space of cubic splines $\mathcal{S}_H \subset C^2(\Omega)$ in order to evaluate weak derivatives up to third order. Furthermore, this already ensures smoothness of the deformations independent of the regularization energy. Here, $H = 2^{-N}$ with $N \in \mathbb{N}$ denotes the grid size of the underlying uniform and quadratic mesh. The associated basis functions are vector-valued B-splines. Moreover, we only impose the Dirichlet boundary condition $\boldsymbol{\Phi} = \mathbb{1}$ on $\partial\Omega$ instead of the stronger boundary conditions $\boldsymbol{\Phi} - \mathbb{1} \in H_0^2(\Omega)$ for the discrete deformations $\boldsymbol{\Phi} \in \mathcal{S}_H$ since we experimentally observed that these Dirichlet boundary conditions appear to be sufficient to reliably compute proper deformations. The gray value images are approximated via finite element functions in the space $\mathcal{V}_h$ of piecewise bilinear and globally continuous functions on Ω with input intensities in the range $[0, 1]$. The underlying grid consists of uniform quadratic cells with mesh size $h = 2^{-M}$ with $M \in \mathbb{N}$ and $M > N$. We take into account the usual Lagrange basis functions and represent image intensities by functions $\mathbf{U} \in \mathcal{V}_h$. In our numerical experiments we set $M = N + 1$.

Now, we are in the position to define spatially discrete counterparts of the operators involved in the fixed point iteration. We apply a Gaussian quadrature of order 5 on both meshes. For the fully discrete counterparts of the operators $\mathcal{T}$ and $\mathcal{R}$ one gets

$$\mathbf{T}[\boldsymbol{\Phi}](\boldsymbol{\Psi}) = \sum_{c_H,q_H} \omega_{q_H}^{c_H} \Big(- 2\gamma((D\boldsymbol{\Phi})^{-T} \circ \boldsymbol{\Phi}_1(\mathbf{x}_{q_H}^{c_H}))D\Delta\boldsymbol{\Phi}_1(\mathbf{x}_{q_H}^{c_H}) : D(\boldsymbol{\Psi} \circ \boldsymbol{\Phi}_1(\mathbf{x}_{q_H}^{c_H}))$$

$$- 2\gamma D\Delta\boldsymbol{\Phi}_1(\mathbf{x}_{q_H}^{c_H}) : D((D\boldsymbol{\Phi})^{-1} \circ \boldsymbol{\Phi}_1(\mathbf{x}_{q_H}^{c_H}))(\boldsymbol{\Psi} \circ \boldsymbol{\Phi}_1(\mathbf{x}_{q_H}^{c_H}))$$

$$- 2\Delta\boldsymbol{\Phi}_1(\mathbf{x}_{q_H}^{c_H}) \cdot ((D\boldsymbol{\Phi})^{-1}\boldsymbol{\Psi}) \circ \boldsymbol{\Phi}_1(\mathbf{x}_{q_H}^{c_H}) \Big)$$

$$- \sum_{c_h,q_h} \frac{\omega_{q_h}^{c_h}}{\delta} \frac{(\mathbf{U}_1 \circ \boldsymbol{\Phi}_1(\mathbf{x}_{q_h}^{c_h}) - \mathbf{U}_0(\mathbf{x}_{q_h}^{c_h}))^2}{\det D\boldsymbol{\Phi}_1(\mathbf{x}_{q_h}^{c_h})}$$

$$\cdot \big((D\boldsymbol{\Phi})^{-T} : (D^2\boldsymbol{\Phi}(D\boldsymbol{\Phi})^{-1}\boldsymbol{\Psi}) - (D\boldsymbol{\Phi})^{-T} : D\boldsymbol{\Psi}\big) \circ \boldsymbol{\Phi}_1(\mathbf{x}_{q_h}^{c_h}) \,,$$

$$\mathbf{R}[\boldsymbol{\Phi}](\boldsymbol{\Psi}) = \sum_{c_H,q_H} \omega_{q_H}^{c_H} \big(2\gamma\Delta\boldsymbol{\Phi}(\mathbf{x}_{q_H}^{c_H}) \cdot \Delta\boldsymbol{\Psi}(\mathbf{x}_{q_H}^{c_H}) + 2D\boldsymbol{\Phi}(\mathbf{x}_{q_H}^{c_H}) : D\boldsymbol{\Psi}(\mathbf{x}_{q_H}^{c_H})\big)$$

for $\boldsymbol{\Psi} \in \mathcal{S}_H$ with $\boldsymbol{\Psi} = 0$ on $\partial\Omega$. Here, we sum over all grid cells c_H of the spline mesh and all local quadrature points within these cells indexed by q_H with respect to the deformation energy and over all grid cells c_h of the finer finite element mesh

and all local quadrature points within these cells indexed by q_h. Here, $(\omega_{q_H}^{cH}, \mathbf{x}_{q_H}^{cH})$ and $(\omega_{q_h}^{ch}, \mathbf{x}_{q_h}^{ch})$ are the pairs of quadrature weights and points on the spline mesh and the finite element mesh, respectively. Moreover, we set $\mathbf{U}_i = \mathcal{I}_h(u_i)$ for $i = 0, 1$ with $\mathcal{I}_h$ representing the Lagrange interpolation on $\mathcal{V}_h$.

Finally, one obtains the following fixed point iteration to compute the spatially discrete deformation $\mathbf{\Phi}_2$

$$\mathbf{\Phi}^{j+1} = \left(\mathbf{R}^{-1} \circ \mathbf{T}\right)[\mathbf{\Phi}^j]$$

for all $j \geq 0$ and initial data $\mathbf{\Phi}^0 = \mathbb{1}$. The application of $\mathbf{R}^{-1}$ requires the solution of the associated linear system of equations. In a preparatory step, the deformation $\mathbf{\Phi}_1 \in \operatorname{argmin}_{\mathbf{\Phi} \in \mathcal{S}_H} \mathbf{W}^D[\mathbf{U}_0, \mathbf{U}_1, \mathbf{\Phi}]$, which is used in the first step of a time discrete geodesic shooting, is calculated using a Fletcher-Reeves nonlinear conjugate gradient descent multilevel scheme with an Armijo step size control.

Then, the deformation in the current step is computed using the aforementioned fixed point iteration, which is stopped if the L^∞-difference of the deformations in two consecutive iterations is below the threshold value $\text{THRESHOLD} = 10^{-12}$. To compute $\mathbf{U}_2$, we employ the spatially discrete analog of the update formula (10)

$$\mathbf{U}_2(\mathbf{x}) = \left(\frac{\mathbf{U}_1 - \mathbf{U}_0 \circ \mathbf{\Phi}_1^{-1}}{\det(D\mathbf{\Phi}_1) \circ \mathbf{\Phi}_1^{-1}}\right) \circ \mathbf{\Phi}_2^{-1}(\mathbf{x}) + \mathbf{U}_1 \circ \mathbf{\Phi}_2^{-1}(\mathbf{x}). \tag{12}$$

Here, we evaluate (12) at all grid nodes of the finite element grid. To compute approximate inverse deformations $\mathbf{\Phi}_i^{-1} \in \mathcal{S}_H$, $i \in \{1, 2\}$, all cells of the grid associated with $\mathcal{S}_H$ are traversed and the deformed positions $\mathbf{\Phi}_i(\mathbf{x}_j)$ for all vertices $\mathbf{x}_j$, $j \in \{1, \ldots, 4\}$, of the current element are computed. Then, we use a bilinear interpolation of these deformed positions to define an approximation of $\mathbf{\Phi}_i^{-1}(x)$ for $x \in \Omega$. Furthermore, we explicitly ensure the boundary condition $\mathbf{\Phi}_i^{-1}(x) = x$ for $x \in \partial\Omega$.

In our numerical experiments on real image data, we observed slight local oscillations emerging from the inexact evaluation of the expression $\mathbf{U}_1(\mathbf{x}) - \mathbf{U}_0 \circ \mathbf{\Phi}_1^{-1}(\mathbf{x})$ in the quadrature of the intensity modulation. Since the calculation of EXP^k requires a recursive application of EXP^2, these oscillations turn out to be sensitive to error propagation, and it is advantageous to apply in each step a post-processing by an anisotropic diffusion filtering (see [9]). Alternatively, one could replace the squared weak material derivative by a term $((1 - \frac{\sigma^2}{2}\Delta)z)^2$ for a small filter width $\sigma << 1$.

6   Numerical results

In this section, we present applications of the fully discrete exponential map proposed in Section 4. In all computations, we used the parameters $\gamma = 10^{-4}$ and $\delta = 10^{-2}$.

In [2, Fig. 6.2], a geodesic sequence between two female portrait paintings[3] was computed using the finite element discretization for both the images and the defor-

---

[3] first painting by A. Kauffmann (public domain, see `http://commons.wikimedia.org/wiki/File:Angelika_Kauffmann_-_Self_Portrait_-_1784.jpg`), second painting by R. Peale (GFDL, see `http://en.wikipedia.org/wiki/File:Mary_Denison.jpg`)
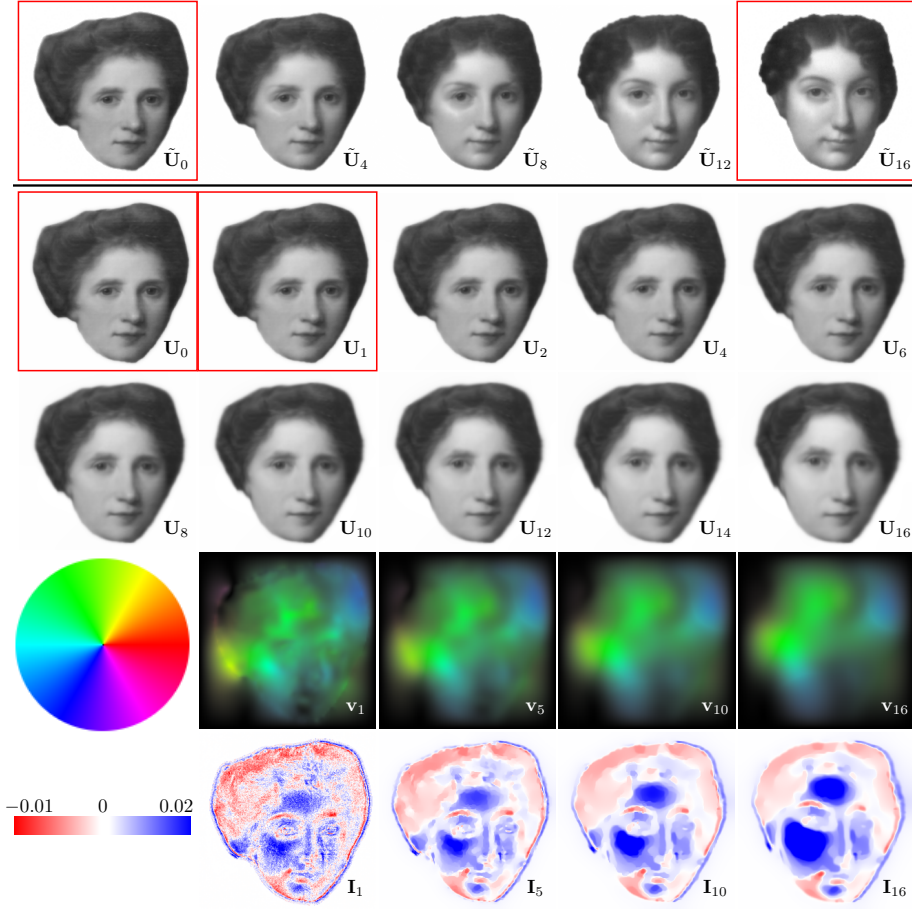
Fig. 2. The first row depicts distinct images of the discrete geodesic sequence associated with the input images $\tilde{\mathbf{U}}_0$ and $\tilde{\mathbf{U}}_{16}$ (in red boxes). The discrete exponential map for distinct time steps is shown in the second and third row, where the input images $\mathbf{U}_0$ and $\mathbf{U}_1$ coincide with $\tilde{\mathbf{U}}_0$ and $\tilde{\mathbf{U}}_1$ from the geodesic sequence, respectively. In addition, the corresponding discrete velocity field as well as the intensity modulation (fourth and fifth row) are shown.

mations on the same grid. The image resolution is 257×257 ($M = 8$). We recomputed this geodesic sequence $(\tilde{\mathbf{U}}_0, \tilde{\mathbf{U}}_1, \ldots, \tilde{\mathbf{U}}_{16})$ with $K = 16$ for the discrete function spaces $\mathcal{V}_h$ and $\mathcal{S}_H$ with $N = 7$, the resulting sequence is shown in the first row of Figure 2 with framed input images $\tilde{\mathbf{U}}_0$ and $\tilde{\mathbf{U}}_{16}$. Afterwards, a discrete exponential shooting was computed with an initial image $\mathbf{U}_0$ and an initial variation $\mathbf{U}_1 - \mathbf{U}_0$ taken from this geodesic sequence. In the fourth and fifth row, the discrete motion field $\mathbf{v}_k = \frac{1}{\tau}(\boldsymbol{\Phi}_k - \mathbb{1})$, which significantly alters in time, and the intensity modulation $\mathbf{I}_k = \mathbf{U}_k \circ \boldsymbol{\Phi}_k - \mathbf{U}_{k-1}$ (postprocessed via anisotropic diffusion) are shown, respec-

tively. Furthermore, Figure 3 illustrates the effect of the anisotropic diffusion filtering on the intensity modulation for $k \in \{4, 8\}$.
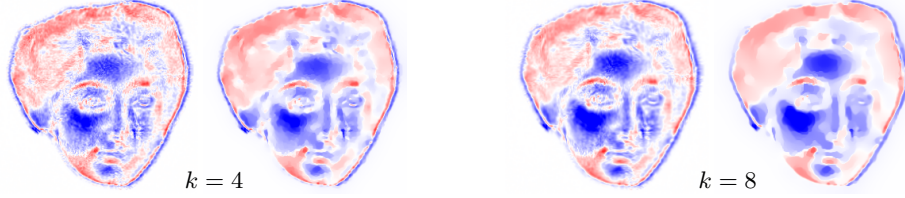

$k = 4$ $k = 8$

Fig. 3. Comparison of the intensity modulations in the application shown in Figure 2 in the case of no post-processing (left) and with the implemented post processing via anisotropic diffusion filtering (right) for $k = 4$ (first image pair) and $k = 8$ (second image pair).

Figure 4 depicts a picture detail of the discrete exponential map for time steps $k = 0, 1, 2, 4, 8, 16$ applied to two pairs of photos of human faces with a resolution of 1025×1025 of the full images. The red boxes indicate input images (first and third row). The input pictures are consecutive photos of a series at 5 and 7 fps, respectively, taken with a digital camera. Due to the higher resolution texture of the images the intensity modulations tend to slightly stronger local oscillations, which are damped with a slightly stronger anisotropic diffusion filtering. We observe that small initial variations result in a nonlinear deformation of the lips (first row) and of the lips, the cheeks and the eyes (third row), respectively. Furthermore, the textures are reliably transported along the sequence. The second and fourth row depict the color coded time varying velocity fields.

Appendix

Here, we derive equation (9) from the system of Euler-Lagrange equations (6), (7) and (8). By using the transformation formula the energy $\mathcal{W}^D$ can be rewritten as follows

$$\mathcal{W}^D[u_1, u_2, \phi_2] = \int_\Omega |D\phi_2 - \mathbb{1}|^2 + \gamma|\Delta^m \phi_2|^2 + \frac{1}{\delta} \frac{(u_2 - u_1 \circ \phi_2^{-1})^2}{\det(D\phi_2) \circ \phi_2^{-1}} \, \mathrm{d}x \, .$$

Now we rewrite the Euler-Lagrange equation (8). To this end, we use that

$$\partial_{\phi_2} \phi_2^{-1}(\psi) = -((D\phi_2)^{-1}\psi) \circ \phi_2^{-1} \, ,$$

which follows by differentiating $(\phi_2 + \epsilon\psi) \circ (\phi_2 + \epsilon\psi)^{-1} = \mathbb{1}$ with respect to ϵ, and that $\partial_A \det(A)(B) = \mathrm{cof}(A) : B$ for $A \in GL(n)$ and $B \in \mathbb{R}^{n,n}$ with $\mathrm{cof}\, A = (\det A)A^{-T}$. Thus, we obtain

$$\int_\Omega 2D\phi_2 : D\psi + 2\gamma\Delta^m \phi_2 \cdot \Delta^m \psi + \frac{2}{\delta}(u_2 - u_1 \circ \phi_2^{-1})\frac{(\nabla u_1 \cdot (D\phi_2)^{-1}\psi) \circ \phi_2^{-1}}{\det(D\phi_2) \circ \phi_2^{-1}}$$

$$+ \frac{(u_2 - u_1 \circ \phi_2^{-1})^2}{\delta(\det D\phi_2)^2 \circ \phi_2^{-1}} \left(\mathrm{cof}\, D\phi_2 : (D^2\phi_2(D\phi_2)^{-1}\psi) - \mathrm{cof}\, D\phi_2 : D\psi \right) \circ \phi_2^{-1} \, \mathrm{d}x = 0 \, .$$
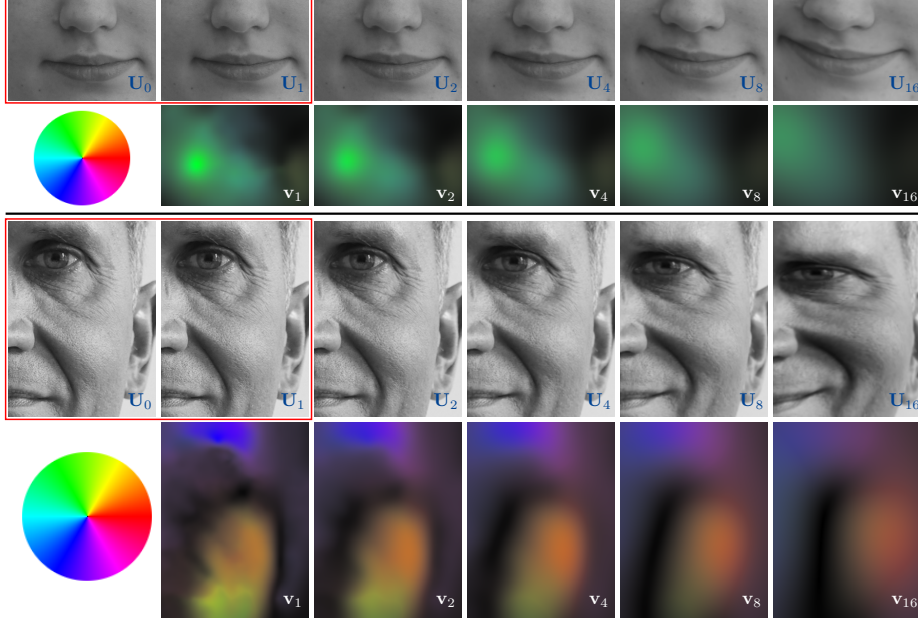
Fig. 4. First/third row: picture details of $\mathrm{EXP}_{\mathbf{U}_0}^k(\mathbf{U}_1 - \mathbf{U}_0)$ applied to two pairs of photos of human faces for the time steps $k = 0, 1, 2, 4, 8, 16$. Second/fourth row: the associated discrete velocity fields $\mathbf{v}_k$.

A further application of the transformation formula with respect to ϕ_2 yields

$$\int_\Omega 2D\phi_2 : D\psi + 2\gamma\Delta^m\phi_2 \cdot \Delta^m\psi + \frac{2}{\delta}(u_2 \circ \phi_2 - u_1)\nabla u_1 \cdot (D\phi_2)^{-1}\psi$$

$$+\frac{1}{\delta}\frac{(u_2 \circ \phi_2 - u_1)^2}{\det D\phi_2}\left(\mathrm{cof}\, D\phi_2 : (D^2\phi_2(D\phi_2)^{-1}\psi) - \mathrm{cof}\, D\phi_2 : D\psi\right)\,\mathrm{d}x = 0. \quad (13)$$

To remove the dependency of the function u_2 above, we employ the pointwise condition

$$u_2 \circ \phi_2 - u_1 = \frac{u_1 - u_0 \circ \phi_1^{-1}}{\det(D\phi_1) \circ \phi_1^{-1}}$$

for a.e. $x \in \Omega$, which directly follows from (6). Inserting this in (13) and using the integral transformation formula we achieve

$$\int_\Omega 2D\phi_2 : D\psi + 2\gamma\Delta^m\phi_2 \cdot \Delta^m\psi + \frac{2}{\delta}(u_1 \circ \phi_1 - u_0)(\nabla u_1 \cdot (D\phi_2)^{-1}\psi) \circ \phi_1$$

$$+\frac{1}{\delta}\frac{(u_1 \circ \phi_1 - u_0)^2}{\det D\phi_1}\left(\frac{\mathrm{cof}\, D\phi_2 : (D^2\phi_2(D\phi_2)^{-1}\psi) - \mathrm{cof}\, D\phi_2 : D\psi}{\det D\phi_2}\right) \circ \phi_1\,\mathrm{d}x = 0.$$

Here, we take into account the identity $\mathrm{cof}(A) = \det(A)A^{-T}$. Next, we consider the test function $\zeta := ((D\phi_2)^{-1}\psi) \circ \phi_1$ in (7). To justify this, we need a regularity result

for polyharmonic PDEs to show $\zeta \in H_0^{2m}(\Omega)$. Inserting ζ into (7) we get

$$-\int_\Omega \frac{2}{\delta}(u_1 \circ \phi_1 - u_0)(\nabla u_1 \cdot (D\phi_2)^{-1}\psi) \circ \phi_1 \, \mathrm{d}x$$

$$= \int_\Omega 2\gamma \Delta^m \phi_1 \cdot \Delta^m(((D\phi_2)^{-1}\psi) \circ \phi_1) + 2D\phi_1 : D(((D\phi_2)^{-1}\psi) \circ \phi_1) \, \mathrm{d}x \, .$$

By adding this identity to the above equation we finally obtain (9).

References

1. M. F. Beg, M. I. Miller, A. Trouvé, and L. Younes. Computing large deformation metric mappings via geodesic flows of diffeomorphisms. *Inter. J. Comput. Vision*, 61(2):139–157, 2005.
2. B. Berkels, A. Effland, and M. Rumpf. Time discrete geodesic paths in the space of images. *SIAM J. Imaging Sci.*, 8 (3):1457–1488, 2015.
3. P. Dupuis, U. Grenander, and M. I. Miller. Variational problems on flows of diffeomorphisms for image matching. *Quart. Appl. Math.*, 56:587–600, 1998.
4. A. Effland, M. Rumpf, S. Simon, K. Stahn, and B. Wirth. Bézier curves in the space of images. In *Proc. of International Conference on Scale Space and Variational Methods in Computer Vision*, volume 9087 of *Lecture Notes in Comput. Sci.*, pages 372–384. Springer, Cham, 2015.
5. D. Holm, A. Trouvé, and L. Younes. The Euler-Poincaré theory of metamorphosis. *Quart. Appl. Math.*, 67:661–685, 2009.
6. W. P. A. Klingenberg. *Riemannian geometry*, volume 1 of *de Gruyter Studies in Mathematics*. Walter de Gruyter & Co., Berlin, second edition, 1995.
7. M. Lorenzi and X. Pennec. Geodesics, parallel transport & one-parameter subgroups for diffeomorphic image registration. *Int. J. Comput. Vis.*, 105(2):111–127, 2013.
8. M. I. Miller and L. Younes. Group actions, homeomorphisms, and matching: a general framework. *Int. J. Comput. Vis.*, 41(1–2):61–84, 2001.
9. P. Perona and J. Malik. Scale-space and edge detection using anisotropic diffusion. *IEEE Transactions on Pattern Analysis and Machine Intelligence*, 12(7):629–639, 1990.
10. M. Rumpf and B. Wirth. Variational time discretization of geodesic calculus. *IMA J. Numer. Anal.*, 35(3):1011–1046, 2015.
11. A. Trouvé. Diffeomorphisms groups and pattern matching in image analysis. *International Journal of Computer Vision*, 28 (3):213–221, 1998.
12. A. Trouvé and L. Younes. Local geometry of deformable templates. *SIAM J. Math. Anal.*, 37(1):17–59, 2005.
13. A. Trouvé and L. Younes. Metamorphoses through Lie group action. *Found. Comput. Math.*, 5(2):173–198, 2005.
14. F.-X. Vialard, L. Risser, D. Rueckert, and C. J. Cotter. Diffeomorphic 3D image registration via geodesic shooting using an efficient adjoint calculation. *International Journal of Computer Vision*, 97:229–241, 2012.
15. F.-X. Vialard, L. Risser, D. Rueckert, and D. D. Holm. Diffeomorphic atlas estimation using geodesic shooting on volumetric images. *Annals of the BMVA*, 2012:1–12, 2012.